Journal of Marine Systems 172 (2017) 84–92

Contents lists available at ScienceDirect

Journal of Marine Systems

journal homepage: www.elsevier.com/locate/jmarsys

The summer-fall anticyclonic eddy west of Luzon: Structure and evolution in 2012 and interannual variability

Xia Wang [a,b,c], Wendong Fang [b,*], Rongyu Chen [b], Shuqun Cai [b]

[a] Guangzhou Institute of Geochemistry, Chinese Academy of Sciences, Guangzhou, China
[b] State Key Laboratory of Tropical Oceanography, South China Sea Institute of Oceanology, Chinese Academy of Sciences, Guangzhou, China
[c] University of Chinese Academy of Sciences, Beijing, China

ARTICLE INFO

Article history:
Received 9 August 2016
Received in revised form 6 March 2017
Accepted 12 March 2017
Available online 16 March 2017

Keywords:
Anticyclonic eddy
Structure and evolution
South China Sea

ABSTRACT

The Conductivity–Temperature–Depth (CTD) and acoustic Doppler current profiler (ADCP) measurements along 18°N off the western Luzon in the South China Sea (SCS), collected during a cruise from August 12–14, 2012, were used to explore the vertical structure of an anticyclonic eddy (AE) during the observational period. Further, the French Archiving, Validation and Interpretation of Satellite Oceanographic data (AVISO) sea level anomaly (SLA) and corresponding anomalous surface geostrophic velocity were used to study the temporal evolution of the AE. The vertical structure of the AE along 18°N in August 2012 showed a trough located near 117.5°E. The AE extended vertically downward and its distinct feature was identifiable to 200 m depth. Seasonal variations of SLA indicate that the AE lasted for 5 months (June to early November), going through the growth and nearly stationary period from mid-June to late August and then propagating westward along 18°N with varying phase speeds and shapes to the continental slope off the southeastern Hainan Island during late September to November. Furthermore, T–S characteristics suggest that the AE was generated off the western Luzon. Interannual variations of the summer (July–September) SLA presented by Empirical Orthogonal Function analysis, indicates that the local circulation was enhanced by the anomalous anticyclonic eddy along 18°N in the years of 2008, 2010, 2012 and 2013 during the period from1993 to 2014.

1. Introduction

The South China Sea (SCS) is the largest semi-enclosed marginal sea in the western Pacific Ocean. Its northeastern region connects to the East China Sea through the Taiwan Strait, and adjoins with the northwestern Pacific via the Luzon Strait (Fig. 1a). The SCS climate is a component of the East Asian monsoon system (Wyrtki, 1961). The upper layer ocean circulation is forced by seasonal monsoon winds, with significant impact of the Kuroshio on the northern region through the Luzon Strait (Fang et al., 1998; Qu, 2000; Qu et al., 2000; Qu, 2001; Xue et al., 2004; Hu et al., 2012). Influenced by the Asian monsoon system, the SCS experiences the northeasterly monsoon in winter and the southwesterly monsoon in summer. In response to the winter monsoon, the upper layer ocean circulation is characterized by a cyclonic gyre. In summer, there are a cyclonic gyre north of about 12°N and an anticyclonic gyre south of about 12°N (Wyrtki, 1961; Qu, 2000; Gan et al., 2006).

The northern SCS is surrounded by Mainland China, Vietnam, Taiwan Island, Luzon Island and Hainan Island (Fig. 1a). Under the combined influence of monsoon winds, the Kuroshio intrusion, complex topography, and tidal forcing, the general circulation is more intricate (e.g., Xue et al., 2004; Fang et al., 2005; Gan et al., 2006). An ocean eddy which is quasi-geostrophic and with horizontal scales of 50–500 km is defined as synoptic eddy (Woods, 1980). Synoptic eddies are relatively active in the northern SCS. They have been receiving more and more attention since the 1990s. Those off the northwestern Luzon have been investigated by a number of previous works (e.g., Li et al., 1998, 2002; Li and Pohlmann, 2002; Yuan et al., 2007; Wang et al., 2008; Chen et al., 2010; Hu et al., 2012; Nan et al., 2011; Zhang et al., 2015). Previous studies showed that most of the northern SCS eddies originated in two areas: one off the southwestern Taiwan and the other off the western Luzon. Wang et al. (2008) examined the origin and evolution of two anticyclonic eddies in the northeastern SCS using multi-satellite remote sensing data, trajectory data of surface drifting buoys, and in situ hydrographic data during winter 2003/2004. Several studies (e.g., Qu, 2000; Yang and Liu, 2003; He et al., 2016) reported that there is a cyclonic eddy (Luzon Cold Eddy) off the western Luzon in winter.

* Corresponding author at: 164 West Xingang Road, Guangzhou 510301, China.
E-mail address: wdfang@scsio.ac.cn (W. Fang).

http://dx.doi.org/10.1016/j.jmarsys.2017.03.004
0924-7963/

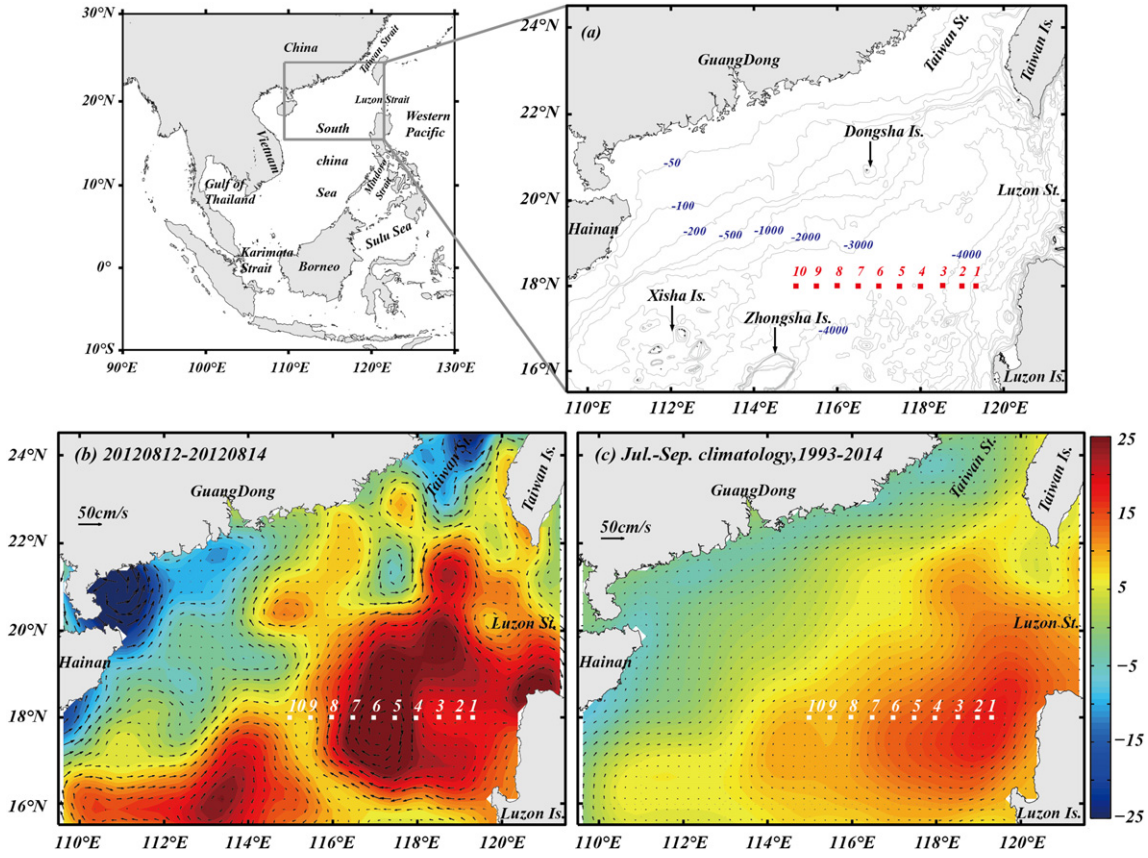

Fig. 1. (a) Observational section and stations from cruise August 2012 and bathymetry of the northern South China Sea (SCS), with the 50, 100, 200, 500, 1000, 2000, 3000, and 4000 m contours plotted. The bathymetry from the ETOPO5 global relief (http://www.ngdc.noaa.gov/mgg/global/etopo5.html) supplied by the National Oceanic and Atmospheric Administration (NOAA) National Geophysical Data Center (NGDC) were used. In situ observational stations are marked by red squares. The detailed information of in situ observation is listed on Table 1. (b) Mean sea level anomaly (SLA, shaded, cm) and the corresponding anomalous surface geostrophic currents (vector, cm·s^{-1}) during the in situ observations from August 12–14, 2012; white squares represent the in situ observational stations. (c) The climatological summer to early fall (July to September) mean SLA (shaded, cm) and anomalous surface geostrophic current (vector, cm·s^{-1}) during 1993–2014 in the northern SCS, showing a sub-basin scale anomalous anticyclonic circulation.

However, to date only a few studies have focused on the summer–fall anticyclonic eddy off the western Luzon. Li et al. (1998) reported that a warm-core anticyclonic eddy occurred off the northwestern Luzon based on CTD (Conductivity–Temperature–Depth) profilers observations. According to that study, the anticyclonic ring originated from Kuroshio meander at the Luzon Strait and shed into the northern SCS. Using satellite altimeter data, Yuan et al. (2007) identified a seasonal anticyclonic eddy generated off the northwest of Luzon, and named it Luzon Warm Eddy (LWE). Chen et al. (2010) investigated the vertical structure and spatiotemporal evolution of the LWE using Argo float data and satellite altimeter data. Based on in situ measurements and satellite sea level anomaly (SLA), Nan et al. (2011) reported three long-lived seasonal anticyclonic eddies occurring along 18°N in August 2007.

Although there are several previous works focused on the anticyclonic eddies off the northwestern Luzon, studies on their hydrographic and current structures from in situ observation, as well as their variation, are still quite scarce. Therefore, this study aims to address the following questions: what is the vertical structure of the anticyclonic eddy? and what is its seasonal evolution and interannual variability? In August 2012, an anticyclonic eddy was captured during the in situ observation along 18°N (see Fig. 1b). In this work, the CTD and acoustic Doppler current profiler (ADCP) measurements along 18°N off the western Luzon in the SCS are used to explore the vertical structure of an anticyclonic eddy (AE) during the observational period of August 12–14, 2012. Further, the AVISO sea level anomaly and corresponding anomalous surface geostrophic currents were employed to study the temporal evolution of the AE. The interannual variability of the eddy activities along 18°N are presented for the first time. Following this introduction, Section 2 describes the data and analysis methods. Section 3 presents the observational results. Section 4 gives a discussion. Finally, Section 5 is the summary.

2. Data and methods

2.1. In situ data and calculation of geostrophic currents

The in situ observation was conducted in August 12–14, 2012 from the R/V Shiyan 3 cruise. Temperature, salinity, density, and sound velocity data were observed using SBE 911plus CTD. There were 10 observational stations along 18°N between 115°E and 119.5°E (Fig. 1a, b). The vertical resolution of the data was 1 m. The observational depths were all greater than 1500 m (Fig. 1a). A vessel–mounted ADCP, made by Teledyne RD Instruments, was used for underway current measurements along the transect. The ADCP current data are available at depths ranging between 38 and 278 m with a vertical interval of 16 m. More detailed information on sampling station and section is listed on Table 1.

In order to calculate the geostrophic currents, the temperature and salinity data from the CTD were processed and interpolated to standard depths consistent with Levitus (1983). By applying the processed CTD data and selecting 1500 m as the reference level, we calculated geostrophic velocities at each standard depth. Pressure gradients below 1500 m are typically weak and the geostrophic currents can be negligible. The validity and effectiveness of such a method to calculate geostrophic currents in the SCS have been demonstrated by previous studies (Fang et al., 2002; Xiang et al., 2016).

Table 1
Details on sampling stations and section of the 2012 cruise.

Item	Date	Station number/section	Measuring instrument	Top/bottom bin depth (m)	Bin size (m)	Sampling interval (min)
CTD	August 12–14	1–10	SBE 911plus	3/1500	1	1
ADCP	August 12–14	18°N	OS38 ADCP	38/278	16	5

2.2. Satellite data and identification of eddies

To identify and track the eddy, daily multi-mission merged SLA (1/4° × 1/4° resolution) and surface geostrophic velocity anomaly (also 1/4° × 1/4° resolution) from the French Archiving, Validation and Interpretation of Satellite Oceanographic data (AVISO) project (http://www.aviso.altimetry.fr/duacs/) were used. The dataset covers the period from 1993 to the present. The climatological summer to early fall (July to September) mean SLA and anomalous surface geostrophic current during 1993–2014 in the northern SCS are shown in Fig. 1c.

The temporal evolution of the eddy was explored using the vector geometry–based detection algorithm (Nencioli et al., 2010). This method used to detect and track eddies is based on the geometry of surface velocities. Its objective is to detect a region where the velocity field rotates around a center. The velocities used in this study are anomalous geostrophic velocities computed from the SLA with the equation for geostrophic equilibrium. The center of the eddy is determined by a

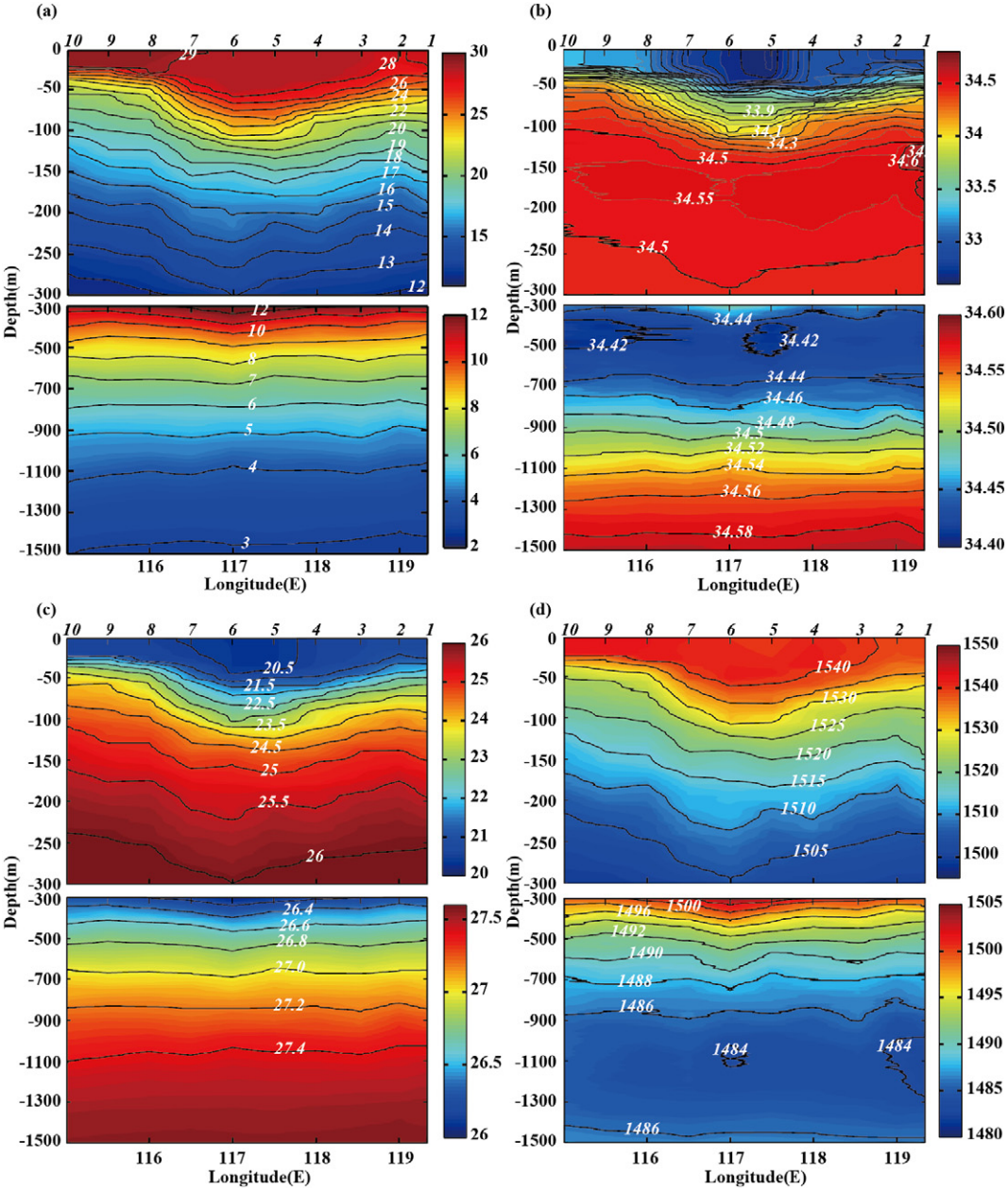

Fig. 2. Vertical distributions of (a) temperature (°C), (b) salinity, (c) density (σ_t; kg·m^{-3}) and (d) sound velocity (m·s^{-1}), along the 18°N section in August 2012.

local velocity minimum in an area where rotating flow has been detected. The eddy boundaries are defined as the outermost one of those closed streamlines around the center, across which velocity is still radially increasing. In order to improve the algorithm performance, the AVISO velocity field was linearly interpolated from a 1/4° × 1/4° grid to 1/8° × 1/8° grid, similar to Liu et al. (2012).

3. Observational results

3.1. Vertical structure of the AE during 12–14 August 2012

Fig. 2 shows the vertical structure of the AE, depicted by vertical sections of temperature, salinity, density and sound velocity from the CTD measurements along 18°N from surface to 1500 m depth. In order to reveal the characteristics of these sectional structures more clearly, we separated the vertical structure into two panels (0–300 m and 300–1500 m). Note that each panel uses a different color scale. The structures of temperature, salinity, density and sound velocity were similar.

A trough was observed in each of the temperature, salinity, density, and sound velocity contour maps, respectively. The troughs were located near 117.5°E (stations 6 and 5), corresponding to the center of the AE at 18°N. The affecting depth of eddy on temperature, salinity, density and sound velocity was about 200 m, indicating that an anticyclonic eddy was present. This AE during the survey period extended vertically downward and its distinct feature was identifiable to 200 m. At the eddy center, the depths of thermocline, pycnocline and sonic layer could have reached 120 m which were 70 m deeper than those (at 50 m depth) in the outermost area of the eddy. The vertical means (0–200 m) of temperature and sound velocity were 2.12 °C and 5.33 cm·s^{-1} larger at the eddy center than those in the surrounding area (station 9 as the reference), respectively, whereas mean salinity and density were 0.25 and 0.78 kg·m^{-3} smaller, respectively.

Fig. 3 shows the vertical distribution of geostrophic current along the 18°N section. The velocity in the west was northward but southward in the east, implying that a distinctive AE existed. The position of the eddy center is generally consistent with the one identified in Fig. 2. The maximum speed was at the surface. The maximum northward speed was ~60 cm·s^{-1}, while the maximum southward speed was 40 cm·s^{-1}.

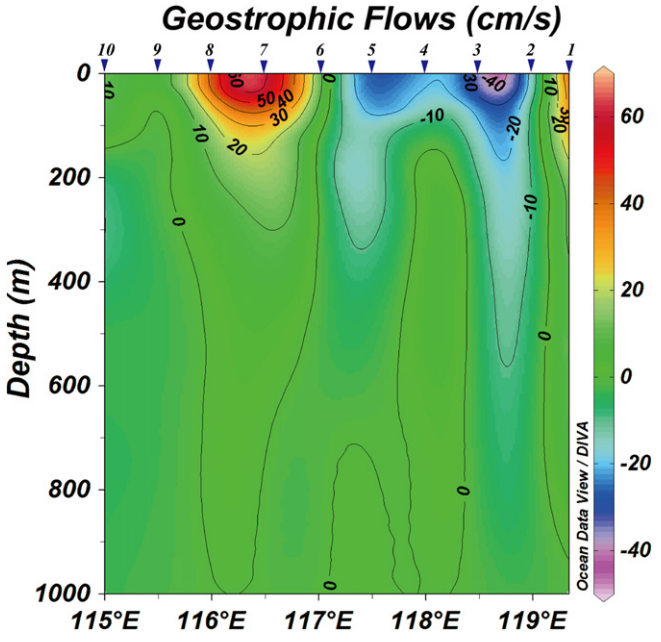

Fig. 3. Vertical distribution of geostrophic current (cm·s^{-1}) along the 18°N section in August 2012. Positive (negative) values represent northward (southward) currents, Data-Interpolating Variational Analysis (DIVA) (Troupin et al., 2012) was used for interpolation.

The depth where the northward speed was over 10 cm·s^{-1} reached nearly 300 m, while the one with southward speed over 10 cm·s^{-1} reached nearly 600 m. The maximum speed during this period is similar to the LWE investigated by Chen et al. (2010). Based on Argo float data from September 2006 to February 2007, Chen et al. (2010) indicated that the LWE extended vertically to more than 500 m depth, with a higher temperature anomaly of 5 °C and lower salinity anomaly of 0.5 near the thermocline. The current speed of the LWE was stronger in its uppermost 200 m, with a maximum speed of 60 cm·s^{-1}.

The currents were also directly measured by the shipboard ADCP along the 18°N section from the cruise. The ADCP current data in 38–278 m is presented in Fig. 4. As depicted in this figure, stronger currents occurred on its western side. Vertically, the eddy had a very similar velocity structure at the depths of 38, 54, and 86 m where the maximum velocity was as high as about 112 cm·s^{-1}, but the velocity gradually weakened below the 86 m layer. The current vectors at the section revealed a clockwise pattern, corresponding to the anticyclonic circulation at 18°N, where the flow was northeastward west of 117°E and southward east of 117.5°E. This was basically consistent with the geostrophic currents although there were some discrepancies in the velocity values, as well as the possible ageostrophic flow included in ADCP currents (Fig. 3).

3.2. Temporal evolution of the AE detected by satellite altimeter data

Fig. 5 shows the temporal evolution of the AE delineated from the surface geostrophic velocity anomaly together with SLA data. The AE was first detected on June 12 off the western Luzon, developed throughout June, intensified in July, started to weaken after the beginning of August, split in September and finally propagated westward to the eastern Hainan Island in early November. The eddy could be traced for nearly five months. The temporal evolution of the AE went through two stages: the growth and quasi-steady period and westward propagation period. The migration speed of the AE in these two stages varied significantly. During the growth and quasi-steady period from mid-June to the end

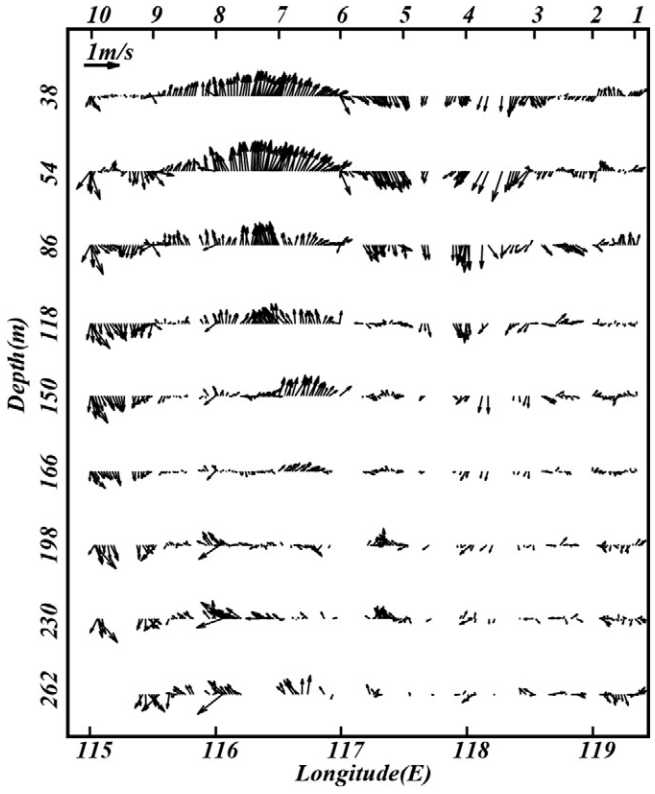

Fig. 4. Current vectors at different depth (as labeled) measured by ADCP for the 18°N section in August 2012. Units in m·s^{-1}.

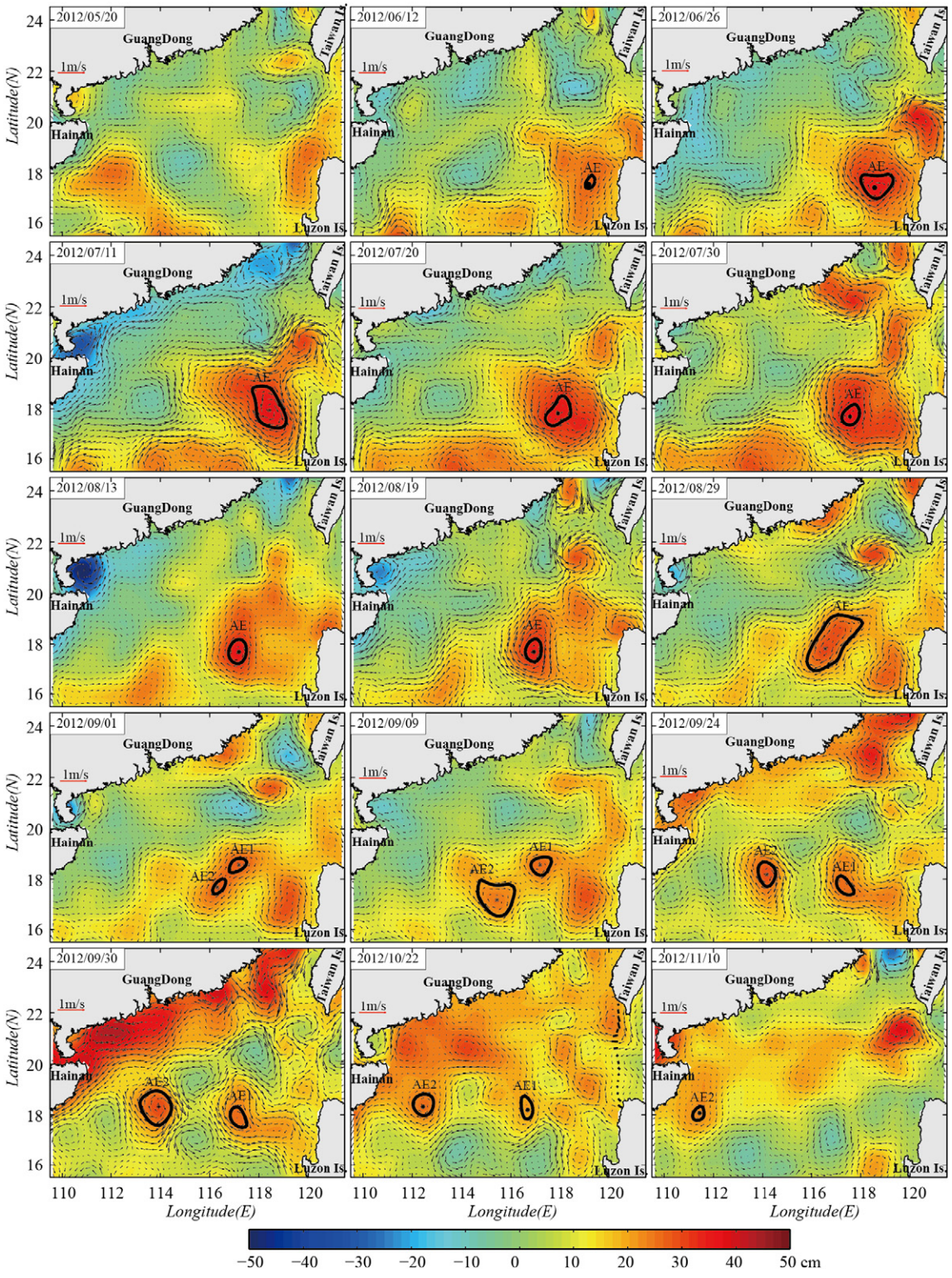

Fig. 5. Temporal evolution of anticyclonic circulation detected by altimeter SLA (color shading, units in cm) and geostrophic currents anomalies (vectors, units in $m \cdot s^{-1}$) from May 20 to November 10, 2012. Closed black lines and black dots denote eddy boundaries and eddy cores, respectively.

of August, the AE started to develop, intensified and weakened. Its diameter varied from 27 to 220 km. The SLA maximum around the eddy center was about 30–40 cm. The westward migration at this stage was relatively slow (less than 4 $cm \cdot s^{-1}$). From September to early November, the AE went through the second stage. The AE split into two anticyclonic eddies (marked as AE1 and AE2 in Fig. 5) in early September. The AE1 and AE2 lasted for about two months. The AE2 migrated westward along section 18°N with a faster speed up to 8 $cm \cdot s^{-1}$, gradually weakened and finally disappeared on the continental slope off the southeastern Hainan Island on November 10. In contrast, the AE1 moved slowly and disappeared on October 22.

The seasonal evolution of the AE in 2012 demonstrated above indicates that the AE migrated westward with varying phase speeds during different stages, consistent with those of previous studies (Yuan et al.,

2007; Chen et al., 2010; Nan et al., 2011). The westward migration speed of the AE was 8.7–14.9 cm·s^{-1} in fall 2002 (Yuan et al., 2007), less than 3.0 cm·s^{-1} in July–September with a faster migration speed of up to14.3 cm·s^{-1} in December (Chen et al., 2010) and 6.0 cm·s^{-1} in September 2007 (Nan et al., 2011).

3.3. Interannual variability of the SLA in July–September

In the SCS, some eddies are seasonal and nearly stationary (e.g., Fang et al., 2002; Xiang et al., 2016) while others clearly propagate like first baroclinic mode Rossby waves (Zhuang et al., 2010; Hu et al., 2012; Lin et al., 2016). By nearly stationary, we mean that the center of the eddy moved somewhat but that the net displacement was small. As presented in Section 3.2, the AE in July–early September had a propagating speed of ~3 km·day^{-1} which is much less than the order of 10 km·day^{-1} for a propagating eddy. Previous study (Chen et al., 2010) indicated that from July to September the moving speed of the AE is very slow (less than 3 cm·s^{-1}). During this period the AE remained nearly stationary off the northwestern Luzon although it translated from late September to winter. Thus, the Empirical Orthogonal Function (EOF) analysis was used to derive the dominant interannual signals during 1993–2014 and the spatial pattern of the July–September SLA variations.

Monthly multi-mission merged SLA (1/4° × 1/4° resolution) from the French AVISO project from 1993 to 2014 was used. To remove the seasonal cycle signal, all the monthly sea level anomalies were derived by departing from their respective climatological mean values averaged over the period of 1993–2014 before the EOF analysis was performed. Finally, the monthly SLA dataset of July–September in 1993–2014 were used for the EOF analysis. The area for the standard EOF analysis was carried out in 113.0°E–121.0°E and 15.5°N–23.0°N.

The first leading EOF mode explained 42.6% of the total variance. This mode has a spatial pattern characterized by two highly positive SLA areas located between 17°N and 20°N, with two maxima centered around 115°E, 18°N and 118°E, 18°N, respectively, corresponding to two eddy-like patterns between 16°N and 20°N (Fig. 6a). The time series of this mode, combined with the spatial pattern, shows the interannual variability of the two eddies. The eastern eddy-like pattern contributes to the variation of the AE. Note that the highest peaks appeared in 2008, 2010, 2012 and 2013, respectively (Fig. 6c). This indicates that SLA was especially high west of Luzon and the two anticyclonic eddies were more energetic during these periods, consistent with the results from our in situ observation in August 2012 as previously noted. Previous study (Nan et al., 2011) showed that two seasonal anticyclonic eddies concurred in summers in some years (e.g., 2007, 2008) in the study area. In addition, the time series of the first EOF mode also displays three phase changes in the years 1998, 2001 and 2006, respectively. Three short term linear trends can be seen from the time series: an increase from 1993 to 2000, a decrease from 2001 to 2004, and a rapid rise for the period 2005–2013. These are similar to the results calculated by Fang et al. (2014), who suggested that the decadal variability of summer circulation in the SCS existed with three phase changes in the years 1998, 2001 and 2006, respectively.

To verify the results from the standard EOF analysis, we also performed a complex EOF analysis which could be used for detection of propagating features with the phase information by using the data set of weekly sea level anomalies of July–September in 1993–2012 (the ending date for weekly SLA data in delay time from the AVISO project is August 2013). The obtained first leading complex EOF mode, explained 32.9% of total variance, shows a distribution of spatial amplitude similar to the first EOF mode with the corresponding spatial nearly uniform phases (not shown). This further confirms that the nearly stationary AE in summer is dominant.

The second EOF mode, which explains 10.4% of the total variance, displayed positive SLAs over the southwest continental slope and negative SLAs southwest of Taiwan Island (Fig. 6b), indicating that another mode exists: two eddy-like patterns out of phase along the continental slope from northeast to southwest.

4. Discussion

4.1. The origin of the AE

As the SCS is a semi-enclosed basin, its water masses differ from those of Pacific Ocean outside the Luzon Strait. In order to verify the

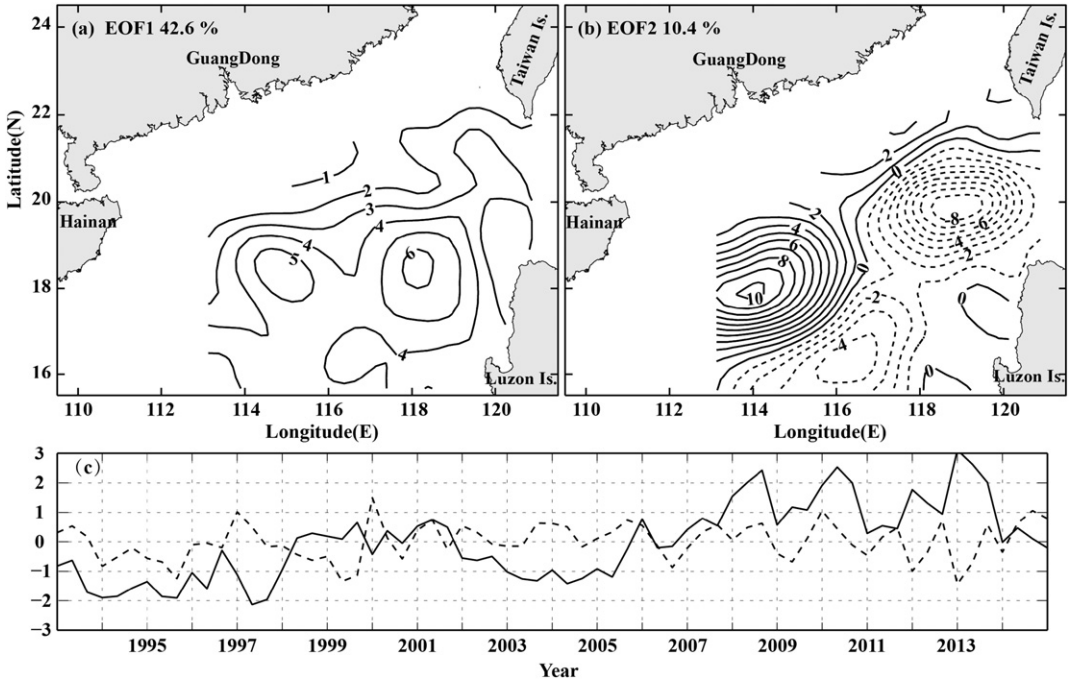

Fig. 6. The first two leading EOF modes of the summer (July–September) SLA, calculated from monthly SLAs with the seasonal signal at summer phase removed; a. spatial pattern of EOF1; b. spatial pattern of EOF2; c. time coefficients of EOF1 (black solid line) and time coefficients of EOF2 (black dotted line).

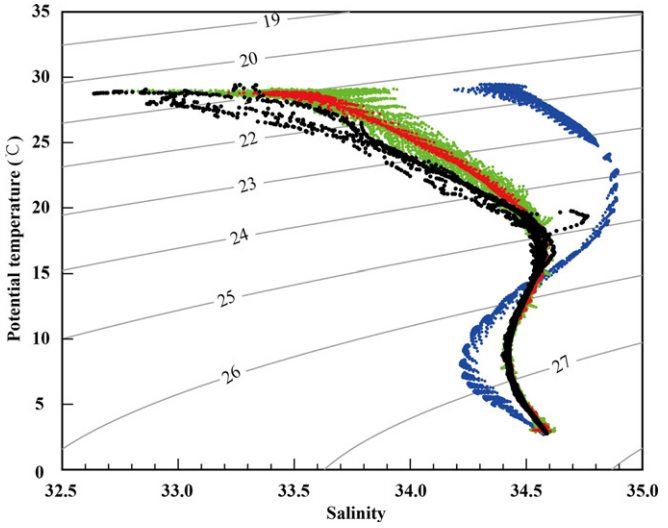

Fig. 7. Potential temperature-salinity scatter diagrams for in situ section data in August 2012 and August climatological data from WOA13. Black points represent data samples at stations 1–10 from in situ data in August 2012. Blue, green and red points represent data samples in the Kuroshio, northern SCS, the area of AE, respectively (temperature and salinity data from WOA2013). Gray contours show potential density $\sigma_{S,\theta,0}$.

origin of the AE, temperature-salinity scatter diagrams for in situ data and August climatological data from the World Ocean Atlas 2013 (WOA13) are shown in Fig. 7. Black points represent data samples at stations 1–10 from in situ observations along the 18°N section in August 2012,whereas blue, green and red points denote data for August climatological T-S scatter diagrams at the east of the Luzon Strait in the Kuroshio region (122.1°E–124.9°E, 19.6°N–20.6°N), the AE region off the western Luzon (116°E–118°E, 17.5°N–18.5°N) and the northern SCS (112.1°E–119.1°E, 16.1°N–18.9°N), respectively. Fig. 7 shows that the water mass characteristics at stations 1–10 were similar. The salinity reached a maximum of 34.6 at 150 m depth where the potential density $\sigma_{S,\theta,0}$was about 25 kg·m^{-3}. Major discrepancies in the T-S characteristics between the SCS and Kuroshio area were the salinity maxima and minima. Originating from the North Pacific Water, the Kuroshio water is more saline with a maximum of about 34.9 east of the Luzon Strait (Nitani, 1972), whereas the maximum salinity in the SCS is usually less than 34.7 (Yang et al., 1988). As depicted in Fig. 7, the maximum salinity of the Kuroshio water reached 34.86–34.89 at 150–200 m depth and the minimum reached 34.19–34.27 at 550–650 m whereas the maximum salinity of the northern SCS water was about 34.56–34.62 at 125–175 m depth with the minimum reaching 34.44–34.47 at 550 m. This indicates that the in situ water temperature and salinity in August off the northwestern Luzon are different from those of the Kuroshio, and the T-S characteristics of the AE are much closer to the northern SCS water whose salinity in the upper layer is much lower than the Kuroshio's (Fig. 7). Qu (2000) suggested that the Kuroshio water east of the Luzon Strait has a salinity maximum exceeding 35.0, while off the western Luzon, water has lower salinity less than 34.58 and is apparently of local origin.

Li et al. (1998) found an anticyclonic eddy centered at about 21°N, 117.5°E just off the continental slope with a horizontal scale of ~150 km in summer 1994. The water characteristics in the AE were between the SCS water and the Kuroshio at the Luzon Strait. The chemical tracer analysis of Li and Pohlmann (2002) suggested that this eddy originates from the Kuroshio. However, based on the SLA and the geostrophic currents from satellite data, Yuan et al. (2007) indicated that the AE originates from northwest of Luzon in early summer. They argued that the anticyclonic eddy discovered by Li et al. (1998) also originated from the northwest of Luzon and primarily carried the SCS water.

In this study, our results showed that the T-S characteristics of the AE are much closer to those of the northern SCS water (Fig. 7). The salinity of the AE was much lower than that of the Kuroshio water, which is consistent with the findings of Yuan et al. (2007). In addition, as shown in Fig. 5, the AE was nearly stationary at an early stage, then propagated westward at varying phase speed and reached the continental shelf area off Hainan Island in early November; During the entire process, the Kuroshio in the Luzon Strait stayed in a path from the northeast of Luzon to the southwest of Taiwan Island, and no significant loop current of the Kuroshio was indicated by the geostrophic currents (not shown). The dominant modes of the Kuroshio path fluctuations in the Luzon Strait consisted of westward intrusion in winter and eastward meandering anomalies in summer (Lin et al., 2016). Recent studies (e.g., Hu et al., 2012) suggested that the eddies in the northeastern SCS have three types of origin: (1) eddies are detached or shed from the Kuroshio, (2) eddies are locally generated in the northeastern SCS, and (3) eddies are generated by the nonlinearity of the Rossby waves from Northwest Pacific and propagate westward into the SCS through the Luzon Strait. Our results suggested that the AE in August 2012 may be generated locally in the SCS.

4.2. Possible mechanisms

In general, eddy extracts energy from the release of the available potential energy (APE) through baroclinic instability, which is stored in the large-scale circulation built up by the wind-driven Ekman pumping (Gill et al., 1974). Physical processes resulting in down-scaled energy transfer could be caused by density fronts, velocity shear or external input of vorticity by wind stress curl (WSC). The dominant response to WSC in the northern SCS is through Ekman pumping modulated by Rossby waves (Xu and Oey, 2015). Recent studies indicated that eddies off the northwest of Luzon were spun up by WSC, embedded in Rossby waves (Lin et al., 2016). In summer, energetic anticyclonic eddies were also observed in the area between 17°N and 19°N off the western Luzon (Nan et al., 2011), much stronger than those in the Luzon Strait due to the Kuroshio retreating eastward in this period; eddies in the area are found to acquire their energy from the mean flow through the release of APE associated with baroclinic instability (Yang et al., 2013). Therefore, the AE may obtain its energy from the local background current via baroclinic instability.

The summer variability in the SCS is strongly affected by the ENSO (El Niño-Southern Oscillation)-associated southwesterly monsoon winds (e.g., Dippner et al., 2007, 2013; Li et al., 2014; Xiang et al., 2016) and on the other hand by the dynamics of North Equatorial Current (NEC) bifurcation via the Luzon Strait (Qu et al., 2000, 2005, 2009; Dippner and Loick-Wilde, 2011). The interannual variability of the AE could be associated with the forcing of local wind and the remote one from West Pacific through oceanic pathway as summarized by Fang et al. (2014). The stronger anticyclonic eddy pattern during 2006–2014 could have been primarily induced by local wind changes within the SCS associated with the ENSO. During strong post-El Niño summers, an anticyclonic WSC anomaly occurs over the central SCS deep basin, strengthening the southerly winds along the western boundary area north of 12°N (Chu et al., 2014; Fang et al., 2014; Li et al., 2014). The southerly winds could force the Vietnamese eastward offshore current shifting northward as the western boundary current instead of separating from the coast (Li et al., 2014). This variability of ocean flow may enhance the northeastward currents in the area between 17°N–19°N, contributing more energy to the local background currents which can cause baroclinic instability, and resulting in stronger anticyclonic eddy activities.

Besides the wind forcing in the SCS, the interannual variation of eddy structures off the western Luzon can be influenced by remote winds in the Pacific Ocean through eastern boundary forcing of the SCS. Remote wind forcing from the tropical Pacific can affect the sea level in the SCS via energy transmission through the Mindoro Strait (e.g., Gordon et al., 2012; Zhuang et al., 2013; Fang et al., 2014). During an El Niño, the NEC

bifurcation shifts to the north resulting in a weaker Kuroshio and favourable inflow through the Luzon Strait into the SCS (Qu et al., 2005). This situation is reversed during La Niña event years (Qu et al., 2009). Thus, during summer months of La Niña years, the southward SCS throughflow is weakened, and even reversed to the north in upper layer along the west coast of Luzon via the Mindoro Strait when less Kuroshio water intrudes into the SCS (Sprintall et al., 2012). The wind-driven baroclinic Rossby waves impinge on the eastern Philippine coast and excite coastal Kelvin waves, conveying the sea level signals through the Mindoro Strait into the eastern SCS. This generates more unstable westward Rossby waves off the western coast of Luzon (Zhuang et al., 2013), which may have contributed to the production of more energetic anticyclonic eddies off the western Luzon during 2006–2010.

5. Summary

Based on in situ sectional measurements of CTD and ADCP in 2012 and satellite altimeter data, we analyzed the vertical structure and evolution of the anticyclonic eddy off the western Luzon during summer–fall 2012. Results in the study showed that the AE in 2012 lasted for five months (June–early November), going through the growth and quasi-steady period from mid-June to late August and then propagating westward along the 18°N pathway with varying phase speeds and shapes to the continental slope off the southeastern Hainan Island. The water mass characteristics revealed by the T-S diagram indicated that the AE might be generated locally in the SCS.

The vertical structure of the AE in August 2012 showed a trough located near 117.5°E. The AE extended vertically downward and its distinct feature is identifiable to 200 m depth. Near the core of the eddy, vertical mean temperature and sound velocity were 2.12 °C and 5.33 $cm \cdot s^{-1}$ larger than those in the surrounding areas, respectively, while mean salinity and density were 0.25 and 0.78 $kg \cdot m^{-3}$smaller, respectively.

Temporal evolution of the long-lived AE in 2012 went through two stages. From June to August, the eddy started to develop and intensify. Its diameter increased from 27 to 220 km and the maximum of sea level anomalies was about 30–40 cm. The westward migration velocity was less than 4 $cm \cdot s^{-1}$. From September on, the AE split into two anticyclonic eddies; one of them had a faster westward migration speed of up to 8 $cm \cdot s^{-1}$, gradually weakened, and finally disappeared off the southeastern Hainan Island in November.

For the first time, interannual variations of the summer (July–September) eddies were presented by EOF analysis, indicating that the local circulation was enhanced by the anomalous anticyclonic eddy along 18°N in the years of 2008, 2010, 2012 and 2013 during the period of 1993–2014.

To date, the dynamics of the summer AE is unknown. Previous studies (e.g., Qu, 2000; Xue et al., 2004; Wang et al., 2008; He et al., 2016) have extensively documented that eddies off the northwestern Luzon in winter can be generated by the WSC. However, the AE in summer off the northwest of Luzon may not be forced by the WSC which is generally positive during this season (Yuan et al., 2007). This paper focused on the spatial structures and its evolution of the AE, as well as its interannual variability in summer. Although possible dynamics of the AE, such as wind stress curl, instability of the Rossby waves, Ekman pumping and instability of the background currents were preliminarily discussed, more detailed mechanisms of the AE's generation and interannual variability need to be intensively explained in future study.

Acknowledgement

This work was supported by the National Science Foundation of China (Nos. 41176025, 41430964). The authors wish to thank the investigators, captain and crew members of R/V Shiyan 3 for the productive cruise in August 2012 which was supported through National Project of Fundamental Work for Science and Technology of China (2008FY110100). We also thank Rong Xiang for assistance in processing the in situ observational data. The altimeter product used in this study was produced by Ssalto/Duacs and distributed by Aviso, with support from Cnes (http://www.aviso.altimetry.fr/duacs/). Comments from two anonymous reviewers helped greatly to improve the manuscript.

References

Chu, X.Q., Xue, H.J., Qi, Y.Q., Chen, G.X., Mao, Q.W., Wang, D.X., Chai, F., 2014. An exceptional anticyclonic eddy in the South China Sea in 2010. J. Geophys. Res. Oceans 119:881–897. http://dx.doi.org/10.1002/2013JC009314.

Chen, G.X., Hou, Y.J., Chu, X.Q., Qi, P., 2010. Vertical structure and evolution of the Luzon Warm Eddy. Chin. J. Oceanol. Limnol. 28:955–961. http://dx.doi.org/10.1007/s00343-010-9040-3.

Dippner, J.W., Bombar, D., Loick-Wilde, N., Voss, M., Subramaniam, A., 2013. Comment on "current separation and upwelling over the southeast shelf of Vietnam in the South China Sea" by Chen et al. J. Geophys. Res. Oceans 118:1618–1623. http://dx.doi.org/10.1002/jgrc.20118.

Dippner, J.W., Loick-Wilde, N., 2011. A redefinition of water masses in the Vietnamese upwelling area. J. Mar. Syst. 84:42–47. http://dx.doi.org/10.1016/j.jmarsys.2010.08.004.

Dippner, J.W., Nguyen, K.V., Hein, H., Ohde, T., Loick, N., 2007. Monsoon-induced upwelling off the Vietnamese coast. Ocean Dyn. 57:46–62. http://dx.doi.org/10.1007/s10236-006-0091-0.

Fang, G.H., Fang, W.D., Fang, Y., Wang, K., 1998. A survey of studies on the South China Sea upper ocean circulation. Acta Oceanogr. Taiwan 37, 1–16.

Fang, W.D., Fang, G.H., Shi, P., Huang, Q.Z., Xie, Q., 2002. Seasonal structures of upper layer circulation in the southern South China Sea from in situ observations. J. Geophys. Res. Oceans 107 (C11):3202. http://dx.doi.org/10.1029/2002JC001343.

Fang, W.D., Shi, P., Long, X.M., Mao, Q.W., 2005. Internal solitons in the northern South China Sea from in situ observations. Chin. Sci. Bull. 50:1627–1631. http://dx.doi.org/10.1360/04wd0361.

Fang, W.D., Qiu, F.W., Guo, P., 2014. Summer circulation variability in the South China Sea during 2006–2010. J. Mar. Syst. 137:47–54. http://dx.doi.org/10.1016/j.jmarsys.2014.04.014.

Gan, J.P., Li, H., Curchitser, E.N., Haidvogel, D.B., 2006. Modeling South China Sea circulation: response to seasonal forcing regimes. J. Geophys. Res. 111, C06034. http://dx.doi.org/10.1029/2005JC003298.

Gill, A.E., Green, J.S.A., Simmons, A.J., 1974. Energy partition in the large-scale ocean circulation and the production of mid-ocean eddies. Deep-Sea Res. 21:499–528. http://dx.doi.org/10.1016/0011-7471(74)90010-2.

Gordon, A.L., Huber, B.A., Metzger, E.J., Susanto, R.D., Hurlburt, H.E., Adi, T.R., 2012. South China Sea throughflow impact on the Indonesian throughflow. Geophys. Res. Lett. 39, L11602. http://dx.doi.org/10.1029/2012GL052021.

He, Y.H., Xie, J.S., Cai, S.Q., 2016. Interannual variability of winter eddy patterns in the eastern South China Sea. Geophys. Res. Lett. 43:5185–5193. http://dx.doi.org/10.1002/2016GL068842.

Hu, J.Y., Zheng, Q.A., Sun, Z.Y., Tai, C.-K., 2012. Penetration of nonlinear Rossby eddies into South China Sea evidenced by cruise data. J. Geophys. Res. 117, C03010. http://dx.doi.org/10.1029/2011JC007525.

Levitus, S., 1983. Climatological atlas of the world ocean. Eos. Trans. AGU 64 (49): 962–963. http://dx.doi.org/10.1029/EO064i049p00962-02.

Li, L., Nowlin, W.D., Su, J.L., 1998. Anticyclonic rings from the Kuroshio in the South China Sea. Deep-Sea Res. I 45:1469–1482. http://dx.doi.org/10.1016/S0967-0637(98)00026-0.

Li, L., Pohlmann, T., 2002. The South China Sea warm-core ring 94S and its influence on the distribution of chemical tracers. Ocean Dyn. 52:116–122. http://dx.doi.org/10.1007/s10236-001-0009-9.

Li, Y.C., Li, L., Lin, M.S., Cai, W.L., 2002. Observation of mesoscale eddy fields in the sea southwest of Taiwan by TOPEX/Poseidon altimeter data. Acta Oceanol. Sin. 24, 163–170 (in Chinese with English abstract).

Li, Y.L., Han, W.Q., Wilkin, J.L., Zhang, W.G., Arango, H., Zavala-Garay, J., Levin, J., Castruccio, F.S., 2014. Interannual variability of the surface summertime eastward jet in the South China Sea. J. Geophys. Res. Oceans 119:7205–7228. http://dx.doi.org/10.1002/2014JC010206.

Lin, Y.C., Oey, L.Y., Wang, J., Liu, K.K., 2016. Rossby waves and eddies observed at a temperature mooring in Northern South China Sea. J. Phys. Oceanogr. 46 (2):517–535. http://dx.doi.org/10.1175/JPO-D-15-0094.1.

Liu, Y., Dong, C.M., Guan, Y.P., Chen, D., McWilliams, J., Nencioli, F., 2012. Eddy analysis in the subtropical zonal band of the North Pacific Ocean. Deep-Sea Res. I 68:54–67. http://dx.doi.org/10.1016/j.dsr.2012.06.001.

Nan, F., He, Z.G., Zhou, H., Wang, D.X., 2011. Three long-lived anticyclonic eddies in the northern South China Sea. J. Geophys. Res. 116, C05002. http://dx.doi.org/10.1029/2010JC006790.

Nencioli, F., Dong, C.M., Dickey, T., Washburn, L., McWilliams, J., 2010. A vector geometry-based eddy detection algorithm and its application to a high-resolution numerical model product and high-frequency radar surface velocities in the Southern California Bight. J. Atmos. Ocean. Technol. 27:564–579. http://dx.doi.org/10.1175/2009JTECHO725.1.

Nitani, H., 1972. Beginning of the Kuroshio. In: Stommel, H., Yashida, K. (Eds.), Kuroshio, Physical Aspects of the Japan Current. Univ. of Wash. Press, Seattle, pp. 129–163.

Qu, T.D., 2000. Upper-layer circulation in the South China Sea. J. Phys. Oceanogr. 30 (6): 1450–1460. http://dx.doi.org/10.1175/1520-0485(2000)030<1450:ULCITS>2.0.CO;2.

Qu, T.D., 2001. Role of ocean dynamics in determining the mean seasonal cycle of the South China Sea surface temperature. J. Geophys. Res. Oceans 106:6943–6955. http://dx.doi.org/10.1029/2000JC000479.

Qu, T.D., Mitsudera, H., Yamagata, T., 2000. Intrusion of the North Pacific waters into the South China Sea. J. Geophys. Res. 105 (C3):6415–6424. http://dx.doi.org/10.1029/1999JC900323.

Qu, T.D., Du, Y., Meyers, G., Ishida, A., Wang, D.X., 2005. Connecting the tropical Pacific with Indian Ocean through South China Sea. Geophys. Res. Lett. 32, L24609. http://dx.doi.org/10.1029/2005GL024698.

Qu, T.D., Song, Y.T., Ymagata, T., 2009. An introduction to the South China Sea throughflow: its dynamics, variability, and application for climate. Dyn. Atmos. Oceans 47:3–14. http://dx.doi.org/10.1016/j.dynatmoce.2008.05.001.

Sprintall, J., Gordon, A.L., Flament, P., Villanoy, C.L., 2012. Observations of exchange between the South China Sea and the Sulu Sea. J. Geophys. Res. 117, C05036. http://dx.doi.org/10.1029/2011JC007610.

Troupin, C., Barth, A., Sirjacobs, D., Ouberdous, M., Brankart, J.-M., Brasseur, P., Rixen, M., Alvera-Azcárate, A., Belounis, M., Capet, A., Lenartz, F., Toussaint, M.-E., Beckers, J.-M., 2012. Generation of analysis and consistent error fields using the Data Interpolating Variational Analysis (DIVA). Ocean Model 52:90–101. http://dx.doi.org/10.1016/j.ocemod.2012.05.002.

Wang, D.X., Xu, H.Z., Lin, J., Hu, J.Y., 2008. Anticyclonic eddies in the northeastern South China Sea during winter 2003/2004. J. Oceanogr. 64:925–935. http://dx.doi.org/10.1007/s10872-008-0076-3.

Woods, J.D., 1980. Do waves limit turbulent diffusion in the ocean. Nature 288, 219–224.

Wyrtki, K., 1961. Physical oceanography of the Southeast Asian waters. Scientific Results of Marine Investigation of the South China Sea and Gulf of Thailand. NAGA Rep. vol. 2. Scripps Inst. of Oceanogr., La Jolla, Calif. (195 pp.).

Xiang, R., Fang, W.D., Zhou, S.Q., 2016. The anticyclonic circulation in the southern South China Sea: observed structure, seasonal development and interannual variability. J. Mar. Syst. 154:131–145. http://dx.doi.org/10.1016/j.jmarsys.2015.10.004.

Xu, F.H., Oey, L.Y., 2015. Seasonal SSH variability of the northern South China Sea. J. Phys. Oceanogr. 45:1595–1609. http://dx.doi.org/10.1175/JPO-D-14-0193.1.

Xue, H.J., Chai, F., Pettigrew, N., Xu, D.Y., Shi, M.C., Xu, J.P., 2004. Kuroshio intrusion and the circulation in the South China Sea. J. Geophys. Res. 109:23. http://dx.doi.org/10.1029/2002JC001724.

Yang, H.J., Liu, Q.Y., 2003. Forced Rossby wave in the northern South China Sea. Deep-Sea Res. I 50:917–926. http://dx.doi.org/10.1016/S0967-0637(03)00074-8.

Yang, H.J., Wu, L.X., Liu, H.L., Yu, Y.Q., 2013. Eddy energy sources and sinks in the South China Sea. J. Geophys. Res. Oceans 118:4716–4726. http://dx.doi.org/10.1002/jgrc.20343.

Yang, Y.H., Li, L., Wang, Z.D., 1988. Characteristics of average T-S, S-Z, and T-Z curves of the South China Sea. Trop. Oceanol. 7 (3), 54–59 (in Chinese with English abstract).

Yuan, D.L., Han, W.Q., Hu, D.X., 2007. Anti-cyclonic eddies northwest of Luzon in summer–fall observed by satellite altimeters. Geophys. Res. Lett. 34, L13610. http://dx.doi.org/10.1029/2007GL029401.

Zhang, W.Z., Xue, H.J., Chai, F., Ni, Q.B., 2015. Dynamical processes within an anticyclonic eddy revealed from Argo floats. Geophys. Res. Lett. 42:2342–2350. http://dx.doi.org/10.1002/2015GL063120.

Zhuang, W., Du, Y., Wang, D.X., Xie, Q., Xie, S.P., 2010. Pathways of mesoscale variability in the South China Sea. Chin. J. Oceanol. Limnol. 28:1055–1067. http://dx.doi.org/10.1007/s00343-010-0035-x.

Zhuang, W., Qiu, B., Du, Y., 2013. Low-frequency western Pacific Ocean sea level and circulation changes due to the connectivity of the Philippine Archipelago. J. Geophys. Res. Oceans 118:6759–6773. http://dx.doi.org/10.1002/2013JC009376.